

Stable Skyrmions in $SU(2)$ Gauged Bose-Einstein Condensates

Takuto Kawakami,¹ Takeshi Mizushima,¹ Muneto Nitta,² and Kazushige Machida¹

¹*Department of Physics, Okayama University, Okayama 700-8530 Japan*

²*Department of Physics, and Research and Education Center for Natural Sciences, Keio University, Kanagawa 223-8521 Japan*

(Dated: July 5, 2018)

We demonstrate that the three-dimensional Skyrmion, which has remained elusive so far, spontaneously appears as the ground state of $SU(2)$ symmetric Bose-Einstein condensates coupled with a non-Abelian gauge field. The gauge field is a three-dimensional analogue of the Rashba spin-orbit coupling. Upon squashing the $SO(3)$ symmetric gauge field to one- or two-dimensional shapes, we find that the ground state continuously undergoes a change from a three-dimensional to a one- or two-dimensional Skyrmion, which is identified by estimating winding numbers and helicity. All of the emerged Skyrmions are physically understandable with the concept of the helical modulation in a unified way. These topological objects might potentially be realizable in two-component BECs experimentally.

PACS numbers: 03.75.Lm, 03.75.Mn, 67.85.Fg, 67.85.Jk

Introduction.— The n -dimensional Skyrmions ($n \leq 3$), classified by the n -th homotopy group ($\pi_n(S^n) = \mathbb{Z}$), have attracted much attention in various research fields, ranging from high-energy to condensed-matter physics [1–3]. It has been demonstrated that the two-dimensional (2D) Skyrmion spontaneously appears as the ground state in helical magnets MnSi and $\text{Fe}_{1-x}\text{Co}_x\text{Si}$ [4–6], a quantum Hall state [7], and continuous vortices analogous to Skyrmions in $^3\text{He-A}$ [8, 9]. Furthermore, it has recently been created by using the phase-imprinting technique in gaseous Bose-Einstein condensates (BECs) [10]. So far those are all 2D objects.

The three-dimensional (3D) Skyrmion is a particlelike soliton in classical field theory, which was hypothetically introduced by Skyrme [1] to describe baryons in a meson field. Although this hypothesis has attracted a lot of attentions for decades, the evidence has yet to be clarified. One difficulty of the proposal is due to the instability of Skyrmions: it is known that in the nonlinear σ -model, the gradient energy makes the 3D Skyrmion unstable toward shrinkage, in spite of the topological stability [1, 3] because energetics differs from topology. To prevent it from shrinkage, Skyrme [1] added *by hand* the quartic differential term, which is the so-called skyrme term. Instead of adding an *ad hoc* Skyrme term, it has been clarified that a non-Abelian gauge field in the form of the t'Hooft-Polyakov monopole, which yields the scaling law the same as the skyrme term, facilitates the stability of the 3D Skyrmion [11]. It is, however, a nonrealistic and purely theoretical proposal, because such a non-Abelian gauge field does not exist in the meson field theory.

On the other hand, the stability of the 3D Skyrmions in multicomponent BECs has been investigated since their proposals [12, 13]. Although the schemes to create and stabilize them [14–19] have theoretically been proposed, the 3D Skyrmion is still elusive both experimentally and theoretically. One reason is that the Skyrmions in previous works are merely metastable solutions of the energy

functional [14–19].

The aim in this Letter is to clarify that a 3D Skyrmion spontaneously emerges as the “ground state” of BECs, coupled with a realistic non-Abelian gauge field, without the help of the Skyrme term. This is the first proposal of the stable Skyrmions with the 3D analogue of Rashba SOCs. First, we demonstrate that the stability of the 3D Skyrmion is physically understandable with the concept of the helical modulation of the order parameter (OP) [20, 21]. We show the phase diagram and the stable Skyrmion textures by numerically solving the full Gross-Pitaevskii (GP) equation. Here, we mainly focus on a BEC with an $SU(2)$ symmetric interaction to capture the essential physics in the presence of the non-Abelian gauge field, as widely studied in the earlier works [14–19]. The Hamiltonian is analogous to the Higgs sector of the Weinberg-Salam model of electroweak interactions [22]. However, we also consider the stability of the 3D Skyrmion against the interaction without $SU(2)$ symmetry.

Recently, there was a major breakthrough that enabled one to artificially imprint a gauge field in ultracold atoms [23–25]. This is intriguing in the sense of accessibility to new topological phases and the appearance of spatially modulated ground states due to non-Abelian gauge fields [28]. The technique is based on the Raman coupling between hyperfine states of atoms which reconstructs the internal degrees of freedom to be degenerate pseudospin states. The Hamiltonian in the pseudospin representation has a fictitious Abelian or non-Abelian gauge field due to the adiabatic motion of its degenerate pseudospin states.

The schemes to generate various types of gauge fields have been proposed theoretically. In two-component BECs, there exist methods to generate 2D and 3D analogues to the Rashba spin-orbit coupling [29–31] and a monopole field with a Dirac string [32]. Recently, the one-dimensional (1D) Rashba+Dresselhaus type gauge

field was experimentally realized by the NIST group [25]. Fermi gases coupled with a non-Abelian gauge field were also investigated [26, 27]. In this Letter, we clarify how such non-Abelian gauge fields stabilize the 3D Skyrmion.

Phase diagram.— We start with the GP energy functional for two-component bosons with the atom mass m and pseudospins \uparrow, \downarrow as

$$E = \mathcal{H}_0 + \int d^3\mathbf{r} \left[\frac{1}{2}r^2n + c_0n^2 + c_1n^2S_z^2 \right], \quad (1)$$

where the particle density is $n(\mathbf{r}) \equiv \Psi_\mu^* \Psi_\mu$ and the \hat{z} -component of the local spin is $S_z(\mathbf{r}) \equiv \frac{1}{2n} \Psi_\mu^* (\sigma_z)_{\mu\nu} \Psi_\nu$. Throughout this Letter, the repeated Greek indices imply the sum on the spin $\mu, \nu, \eta = \uparrow, \downarrow$ and we use the unit of $\hbar = m = \omega = 1$, where ω is the trap frequency. The $c_0 + c_1$ is the interaction strength between bosons in the same pseudospin component and the c_1 indicates the interaction between the intercomponents. The OP Ψ_μ for the condensate obeys the normalization condition, $\int \Psi_\mu^* \Psi_\mu d^3\mathbf{r} = 1$. The single particle Hamiltonian \mathcal{H}_0 in Eq. (1) is given by

$$\mathcal{H}_0 = \int d^3\mathbf{r} [\mathbf{D}_{\mu\nu} \Psi_\nu(\mathbf{r})]^\dagger \cdot [\mathbf{D}_{\nu\eta} \Psi_\eta(\mathbf{r})]. \quad (2)$$

Here, we set the covariant derivative $\mathbf{D}_{\mu\nu} = (-i\nabla\sigma_0 + \mathbf{A})_{\mu\nu}$ with the 2×2 unit matrix σ_0 and a non-Abelian gauge field \mathbf{A} . In most of this Letter, we set $c_1 = 0$ in Eq. (1), which ensures the $SU(2)$ symmetry of the interaction. However, we will mention later that the finite c_1 does not make the Skyrmion unstable.

First of all, we summarize in Fig. 1(a) the schematic phase diagram of BECs coupled with the 3D non-Abelian gauge field,

$$\mathbf{A} = \kappa_\perp (\sigma_x \hat{\mathbf{x}} + \sigma_y \hat{\mathbf{y}}) + \kappa_z \sigma_z \hat{\mathbf{z}}, \quad (3)$$

where σ_j denotes the j -th Pauli matrix. This is 3D analogue of a Rashba or Dresselhaus type spin-orbit coupling which is known in the condensed matter context. In fact, the scheme to generate this type of synthetic gauge field with $\kappa_z = \kappa_\perp$ [31] and $\kappa_z = 0$ [29, 30] was proposed theoretically, and the case of $\kappa_\perp = 0$ was realized in the experiment [25] as mentioned. In Fig. 1(a), we find out the stable region of the 3D Skyrmion texture, while the other regions are occupied by the 1D or 2D Skyrmion. It turns out that these textures smoothly change to each other. It is demonstrated in the rest of this Letter that all types of Skyrmions, whose textures are displayed in Fig. 2 are understandable with the helical modulation of the OP which can be parameterized on the three-dimensional surface S^3 in the OP space.

Helical spin modulation and Skyrmions.— The concept of the helical modulation of the OP [21] provides a good starting point to the understanding of the stability and smooth transition of Skyrmions under the non-Abelian gauge field described in Eq. (3).

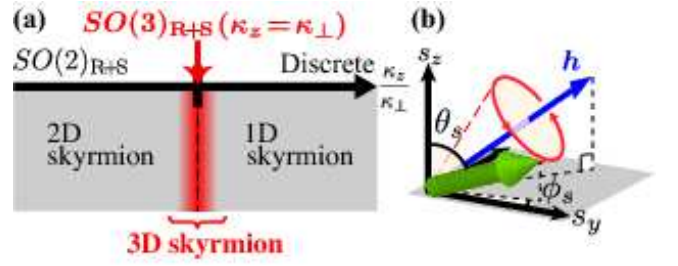


FIG. 1: (Color online) (a) Schematic phase diagram of textures and the symmetries of \mathcal{H}_0 . At $\kappa_z = \kappa_\perp$, the Hamiltonian has an $SO(3)_{R+S}$ symmetry. (b) Schematic picture of the helical spin modulation along \mathbf{h} . The thick green (gray) arrow depicts the local spin $S_j^{(0)} \equiv \frac{1}{2} \{ \Psi_\mu^{(0)}(\mathbf{r}_0) \}^* (\sigma_j)_{\mu\nu} \Psi_\nu^{(0)}(\mathbf{r}_0) / n(\mathbf{r}_0)$.

The OP of a two-component BEC is always parameterized, the $U(1)$ phase $\Phi \equiv \Phi(\mathbf{r})$, and the angles $\phi_s \equiv \phi_s(\mathbf{r})$ and $\theta_s \equiv \theta_s(\mathbf{r})$, as

$$\begin{pmatrix} \Psi_\uparrow(\mathbf{r}) \\ \Psi_\downarrow(\mathbf{r}) \end{pmatrix} = \sqrt{n(\mathbf{r})} e^{i\Phi} e^{-i\sigma_z \phi_s / 2} e^{-i\sigma_y \theta_s / 2} \begin{pmatrix} 1 \\ 0 \end{pmatrix}. \quad (4)$$

Here, as shown in Fig. 1(b), $\phi_s(\mathbf{r})$ and $\theta_s(\mathbf{r})$ denote the direction of the local spin, $S_j(\mathbf{r}) \equiv \frac{1}{2} \Psi_\mu^*(\mathbf{r}) (\sigma_j)_{\mu\nu} \Psi_\nu(\mathbf{r}) / n(\mathbf{r})$. Since the OP manifold in Eq. (4) is mapped onto a three-dimensional surface $SU(2) \simeq S^3$, two-component BECs have a topological object classified by the homotopy group $\pi_3(S^3) = \mathbb{Z}$.

Turning now to a non-Abelian gauged BEC, we demonstrate that the helical modulation of the OP due to the field \mathbf{A} makes the Skyrmion stable even without the Skyrme term. It is crucial to observe that the helical modulation with an arbitrary modulation vector \mathbf{h} can be written down within the $SU(2)$ symmetric OP in Eq. (4) as

$$\Psi_\mu^H(\mathbf{r}, \mathbf{h}) = \mathcal{U}_{\mu\nu}(\hat{\mathbf{h}}, 2\mathbf{h} \cdot \mathbf{r}) \Psi_\nu^{(0)}(\mathbf{r}_0), \quad (5)$$

where the 2×2 matrix $\mathcal{U}(\hat{\mathbf{n}}, \varphi) = \exp[i(\varphi/2)(\hat{\mathbf{n}} \cdot \boldsymbol{\sigma})] \in SU(2)$ denotes the $SU(2)$ rotation of an arbitrary OP $\Psi_\mu^{(0)}$ around $\hat{\mathbf{n}}$ by the angle φ . Figure 1(b) shows the schematic picture of this modulation. The helicity originates from the single particle spectrum $E_0 = \mathcal{H}_0$ of ideal Bose gases in the thermodynamic limit $\Psi_\mu(\mathbf{r}) = e^{i\mathbf{k} \cdot \mathbf{r}} \Psi_\mu^{(0)}$, which is given by $E_0 = k^2 + \kappa^2 \pm 2\sqrt{\kappa_z^2 k_z^2 + \kappa_\perp^2 (k_x^2 + k_y^2)}$ with $\kappa^2 = \kappa_z^2 + 2\kappa_\perp^2$. It turns out that the OP of the ground state is spatially modulated, since E_0 has minima on the finite \mathbf{k} . Then, the helical modulation with $\hat{\mathbf{h}}$ in Eq. (5) is the superposition of momentum eigenstates $\mathbf{k} \parallel \pm \mathbf{h}$. The spatial inversion symmetry of \mathcal{H}_0 guarantees the degeneracy of the helical modulation starting from an arbitrary $\Psi_\mu^{(0)}$.

For $\kappa_z = \kappa_\perp = \kappa/\sqrt{3}$, the single particle Hamiltonian \mathcal{H}_0 in Eq. (1) is invariant under the simultaneous rotation of spin and real spaces $SO(3)_{R+S}$. Since E_0 has

minima on surface $k = \kappa/\sqrt{3}$, the helical spin modulation in Eq. (5) is degenerate for any direction of $\hat{\mathbf{h}} \parallel \hat{\mathbf{k}}$. Note that the 3D helical modulation $\Psi_\mu^{\text{H}}(\mathbf{r}, \mathbf{h} \parallel \mathbf{r})$ propagating with all the directions of \mathbf{h} along \mathbf{r} fulfills the OP manifold S^3 within $0 \leq \mathbf{h} \cdot \mathbf{r} \leq \pi$. Thus, this texture $\Psi_\mu^{\text{3D}} \equiv \Psi_\mu^{\text{H}}(\hat{\mathbf{r}}, 2\mathbf{h} \cdot \mathbf{r})$ is the 3D Skyrmion, which is the candidate of the ground state.

In contrast, for the region $\kappa_z/\kappa_\perp < 1$ in Fig. 1(a), the $SO(3)_{\text{R+S}}$ symmetry in \mathcal{H}_0 in Eq. (1) is broken into the $SO(2)_{\text{R+S}}$ that denotes the joint rotation of spin and real spaces around the $\hat{\mathbf{z}}$ -axis. E_0 also has a minimum line along $k_\perp \equiv \sqrt{k_x^2 + k_y^2} = \kappa_\perp$. Therefore, it turns out that the possible stable texture for $\kappa_z < \kappa_\perp$ is the radial or the 1D helical spin modulation expressed by Eq. (5) with $\mathbf{h} \parallel (k_x, k_y, 0)$, where the former corresponds to a 2D Skyrmion [34].

For the region $\kappa_z/\kappa_\perp > 1$ in Fig. 1(a), the Hamiltonian (1) still remains invariant under the discrete symmetry that is the simultaneous π -rotation of spin and real spaces around the $\hat{\mathbf{x}}$ - or $\hat{\mathbf{y}}$ -axis, where E_0 has minima at $\mathbf{k} = \pm\kappa_z\hat{\mathbf{z}}$. Then the most stable modulation vector \mathbf{h} is confined to the $\hat{\mathbf{z}}$ -axis, implying that the possible stable texture is the 1D helical modulation along $\hat{\mathbf{z}}$ -axis. Since this spin-rotation along the $\hat{\mathbf{z}}$ -axis consists of the $U(1)$ degrees of freedom, we can interpret this helical spin modulation as a 1D Skyrmion.

Stable Skyrmion textures.— In order to quantitatively discuss the candidates of the stable spin textures, we numerically minimize the full Gross-Pitaevskii energy functional (1) by using the imaginary time evolution scheme [33] with a spatial grid of 121^3 . We have verified that the obtained solution is the true ground state by starting the calculation from a variety of initial conditions such as the uniform spin, helical modulation with a variety of modulation vectors, and 2D and 3D Skyrmions. For numerical calculations, we use $c_0 = 100$, where the density profile yields a Gaussian-like shape. This parameter corresponds to the trap frequency $\omega/2\pi = 100$ Hz and s -wave scattering length of the same component $a_{11} = a_{22} = 5$ nm with the ^{87}Rb mass and number of trapped atoms $N = 5 \times 10^4$. These values define the length of the trap unit as $\sqrt{\hbar/m\omega} \simeq 1$ μm . To quantify the size of the atomic cloud, we use the Thomas-Fermi radius $R_0 = \sqrt{2\mu_0} = 2.99$ in the trap unit, where $\mu_0 = (15c_0/2\pi)^{2/5}/2$ is the chemical potential with the Thomas-Fermi approximation.

Figure 2 shows the stable 3D Skyrmion obtained from the numerical minimization of Eq. (1) in the presence of the gauge field with $\kappa_\perp = \kappa_z$ and the spherical trap potential. Figure 2(a) shows that the pseudospin texture helically modulates along the 3D radial direction. In this texture, the singularity of the $U(1)$ phase Φ and the angle ϕ_s introduced in Eq. (4) exists on the gray line where the local spin points to $\hat{\mathbf{z}}$ (Ψ_\downarrow -singularity) or $-\hat{\mathbf{z}}$ (Ψ_\uparrow -singularity) direction. As shown in Fig. 2(b) and 2(c),

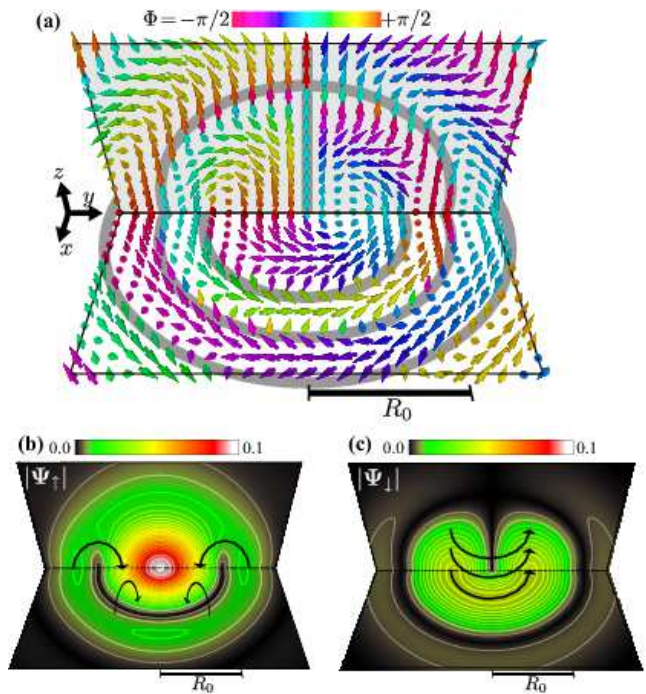


FIG. 2: (Color online) The spatial profile of the stable 3D Skyrmion in the $\hat{\mathbf{x}}\text{-}\hat{\mathbf{y}}$ and $\hat{\mathbf{z}}\text{-}\hat{\mathbf{x}}$ planes. The arrows and their colors in (a) indicate the pseudospin direction and the $U(1)$ phase of the OP, respectively. The gray lines in (a) imply the singularity of Φ and ϕ_s . The color maps of (b) and (c) give the amplitudes $|\Psi_\uparrow(\mathbf{r})|$ and $|\Psi_\downarrow(\mathbf{r})|$, respectively. The black arrows in (b) and (c) denote the directions of the phase winding of each component. These results are obtained with the parameter $(\kappa_\perp R_0, \kappa_z R_0) = (5.07, 5.07)$, where $R_0 = (15c_0/2\pi)^{1/5}$.

OP component Ψ_μ accumulates the phase 2π on the path enclosing its singularity. Namely, Ψ_\uparrow forms the vortex ring and its ring-singularity is fulfilled by Ψ_\downarrow with the phase winding. This can be interpreted as the so-called “vorton” structure known in high-energy physics [8, 35].

The 3D Skyrmion is identified by the winding number $\pi_3(S^3)$ of the map from real space to the OP manifold $SU(2) \simeq S^3$. The winding number defined by Refs. [1, 14–17]

$$W_{3\text{D}} = \frac{1}{8\pi^2} \int d^3\mathbf{r} \epsilon_{ijk} \sin\theta_S (\partial_i\theta_S)(\partial_j\phi_S)(\partial_k\Phi) \quad (6)$$

counts how many times the map warps the OP manifold. Figure 3(a) shows the winding number $W_{3\text{D}}$ in the plane of κ_z/κ_\perp and $R_0\kappa_\perp$, obtained from the numerical solution of the full GP equation. Here, we estimate Eq. (6) in the region of $r \leq 1.5R_0$. It is seen from Fig. 3(a) that $W_{3\text{D}}$ increases with growth of the κ_\perp/R_0 near the $\kappa_z/\kappa_\perp = 1$ line. Hence, in this region the 3D Skyrmion becomes stable. This continuous increase of $W_{3\text{D}}$ is because of the absence of the boundary condition that $\Psi_\mu(\mathbf{r} \rightarrow \infty)$ is nonzero and uniform, assumed for Skyrmions in other contexts. So far as the bound-

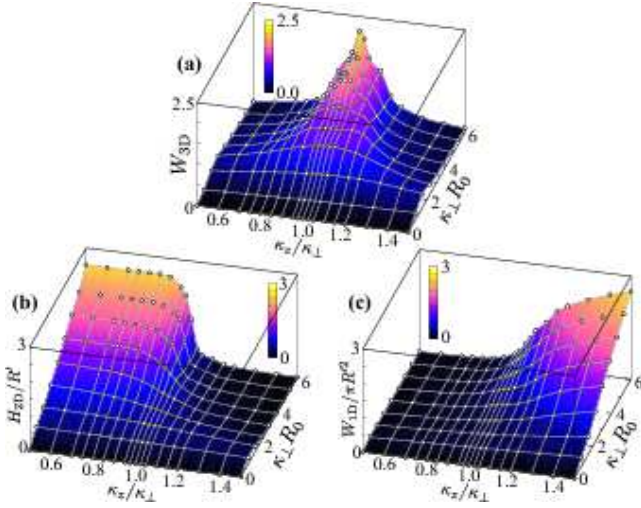


FIG. 3: (Color online) Stereographic plots of W_{3D} (a), H_{2D}/R' (b), and $W_{1D}/\pi R'^2$ (c) in the plane of κ_z/κ_\perp and $\kappa_\perp R_0$. These denote the winding numbers and helicity which quantify the 1D, 2D, and 3D Skyrmions. We estimate these values in the region of $r \leq 1.5R_0 \equiv R'$.

any condition is satisfied, $W_{3D} \in \mathbb{Z}$ and 3D Skyrmion is topologically stable. However, the presence of the vector potential \mathbf{A} makes $\Psi_\mu(\mathbf{r} \rightarrow \infty)$ nonuniform even if we ignore the effect of the trap. In fact, with increasing of $\kappa_z = \kappa_\perp \gtrsim R_0^{-1}$, the characteristic length of the helical spin modulation becomes smaller and the shell-shaped Skyrmion penetrates from outside of the system in addition to a unit of the Skyrmion. Therefore, as κ increases, W_{3D} increases continuously and monotonically as shown in Fig. 3(a).

One- and two-dimensional Skyrmions.— The 2D Skyrmion texture is described as $\Psi_\mu^{2D} = \Psi_\mu^H(\mathbf{r}, \mathbf{h} \parallel \boldsymbol{\rho})$, where $\boldsymbol{\rho} = \mathbf{x} + \mathbf{y}$. The Skyrmion Ψ_μ^{2D} consists of the helical spin modulation along the 2D radial direction, which is favored by the gauge field described in Eq. (3) as mentioned above. This texture occupies the region $\kappa_z/\kappa_\perp \lesssim 1$ in Fig. 1(a). If we ignore the $U(1)$ phase Φ , the winding number of this 2D Skyrmion can be defined as $W_{2D} = \frac{1}{4\pi} \int d^3\mathbf{r} \epsilon_{ij} \sin \theta_S (\partial_i \theta_S) (\partial_j \phi_S)$ [34].

We should notice that the winding number of Ψ_μ^{2D} is determined by the domain of the rotating angle Ω ; $W_{2D} = +1$ (-1) is accumulated within $n\pi < \Omega < (n+1/2)\pi$ ($(n-1/2)\pi < \Omega < n\pi$). This implies that with increasing κ_\perp , the Skyrmion ($W_{2D} = +1$) and anti-Skyrmion ($W_{2D} = -1$) penetrates from outside alternately. Hence, W_{2D} of 2D Skyrmion Ψ_μ^{2D} oscillates with increasing κ_\perp . Instead of W_{2D} , one can estimate the size of the 2D Skyrmion with the helicity introduced as $H_{2D} = \frac{1}{4\pi} \int d^3\mathbf{r} |\epsilon_{ij} \sin \theta_S (\partial_i \theta_S) (\partial_j \phi_S)|$.

The 1D Skyrmion along the \hat{z} -axis is described as $\Psi_\mu^{1D} = \Psi_\mu^H(\mathbf{r}, \mathbf{h} \parallel \hat{z})$. This appears as the ground state in the region $\kappa_z/\kappa_\perp \gtrsim 1$ of Fig. 1(a), where the modulation vector $\mathbf{h} \propto \pm \kappa_z \hat{z}$ is favored as discussed above. The

winding number for the 1D Skyrmion is introduced as $W_{1D} = \frac{1}{2\pi} \int dz \frac{\Psi_\mu^* \partial_z (\sigma_z)_{\mu\nu} \Psi_\nu}{\Psi_\mu^* \Psi_\mu} + \text{c.c.}$. This corresponds to the phase accumulation which quantifies the spin current of S_z along \hat{z} -axis.

We plot W_{1D} and H_{2D} in Figs. 3(b) and (c), where they reveal the stable region of the 1D and 2D Skyrmions in the parameter space spanned by κ_z and κ_\perp . In the region $\kappa_z/\kappa_\perp \lesssim 1$, the 2D Skyrmion is stabilized where the helicity H_{2D} increases and W_{3D} and W_{1D} are suppressed. In the other region, $\kappa_z/\kappa_\perp \gtrsim 1$, the growth of W_{1D} and the suppression of W_{3D} and H_{2D} indicate the appearance of the 1D Skyrmion. Figure 3 provides evidence of the schematic phase diagram in Fig. 1(a).

Three types of Skyrmions can be continuously transformed into each other and the transition between them is identified as the second-order transition. The cylindrical singularity of the component Ψ_\uparrow and Ψ_\downarrow in the 2D Skyrmion continuously deforms to sphere and ring-shaped ones and then the texture changes into the 3D Skyrmion. This is confirmed by the imaginary time evolution of the GP functional (1), which demonstrates that the 2D Skyrmion state becomes unstable in the vicinity of $\kappa_z/\kappa_\perp \sim 1$ toward the 3D Skyrmion. The 3D Skyrmion state also becomes unstable in the region of $\kappa_z/\kappa_\perp \gtrsim 1$, where the singular line and sphere of Ψ_\uparrow described in Fig. 2(a). Hence, the 2D Skyrmion solution smoothly transforms to 1D Skyrmion through the 3D Skyrmion as κ_z/κ_\perp varies from $+0$ to $+\infty$, and the 3D Skyrmion texture spontaneously appears at $\kappa_z/\kappa_\perp \simeq 1$.

We emphasize that the smooth transition behavior between Skyrmions ensures the stability region of the 3D Skyrmion against finite $c_1 \neq 0$, which breaks the $SU(2)$ symmetry in Eq. 1. This is because the stability of 1D and 2D Skyrmions in the limit $\kappa_z \rightarrow 0$ and $\kappa_\perp \rightarrow 0$ stays unchanged in $c_1 \neq 0$ [20, 36]. In fact, within $0 < c_1/c_0 \lesssim 1$, we numerically confirm that the winding number W_{3D} increases as approaching $\kappa_z/\kappa_\perp \rightarrow 1$ and the 3D Skyrmion $\Psi^{3D} = \mathcal{U}_{\mu\nu}(\hat{\mathbf{r}}, 2\kappa r) \Psi_\mu^{(0)}$ with $(\Psi_\uparrow^{(0)}, \Psi_\downarrow^{(0)}) = (1, 0)$ is stabilized. In the case of $c_1/c_0 < 0$, the 3D Skyrmion with $(\Psi_\uparrow^{(0)}, \Psi_\downarrow^{(0)}) = (1, 1)$ is also stabilized.

Skyrmions in other systems.— The stability of the 3D Skyrmion in other spinor systems is worth a mention in passing. For instance, we find that the 3D gauge field in Eq. (3) cannot stabilize the 3D Skyrmion in the polar phase of a hyperfine spin $F=1$ spinor BEC, which is the “knot” soliton. This is because the helical modulation of the polar OP is not degenerate for the 3D direction of the modulation vector [38, 39]. In fact, the OP manifold in the polar phase reduces to an $SO(2)$ symmetry in spin space. Hence, since the helical modulation vector along the direction of the $SO(2)$ rotation axis cannot gain the single particle energy E_0 , only the 2D or 1D Skyrmion can be stable in this system. In the ferromagnetic phase of an $F=1$ spinor BEC, the 1D Skyrmion [20] and the 2D half-Skyrmion [37] are proposed. However, the problem

on the stability of the 3D Skyrmion remains as nontrivial.

Conclusions.— Here, we have demonstrated that the 3D Skyrmion spontaneously appears as the ground state of two-component BECs coupled with a non-Abelian gauge field, which is a 3D analogue of the Rashba spin-orbit coupling. The appropriate gauge field and the spherical density distribution due to the trap potential are necessary to stabilize the Skyrmions. Upon squashing the 3D gauge field to 1D or 2D shape, the 3D Skyrmion continuously undergoes a change to 1D or 2D Skyrmion. We computed the ground state phase diagram with the winding numbers and helicity, which is covered by three types of Skyrmions. All of the emerged Skyrmions are understandable with the concept of the helical modulation of the order parameter. In addition to the $SU(2)$ symmetric interaction, we also consider the stability of Skyrmions against an $SU(2)$ nonsymmetric interaction. Then, we confirmed that the asymmetric term does not alter the phase diagram. However, the interaction in the presence of a synthetic gauge field depends on the detail of the scheme to imprint it. The complete phase diagram in the more realistic situation remains as a future problem.

The authors thank Sankalpa Ghosh and M. Ichioka for helpful discussions. This work was supported by JSPS (No. 2200247703, 2074023303, 23740198, 2134010303) and the Topological Quantum Phenomena (No. 22103005, 23103515) KAKENHI on Innovation areas from MEXT.

Note added.— After we submitted this paper, we became aware of two papers [40, 41] which discuss the ground state properties under the same gauge field.

-
- [1] T. H. R. Skyrme, Proc. R. Soc. A **260**, 127 (1961); Nucl. Phys. **31**, 556 (1962).
- [2] *The Multifaceted Skyrmion*, edited by G. E. Brown and M. Rho (World Scientific, Singapore, 2010).
- [3] I. Zahed and G. E. Brown, Phys. Rep. **142**, 1 (1986).
- [4] U. K. Röbber, A. N. Bogdanov, and C. Pfeleiderer, Nature **442**, 797 (2006).
- [5] S. Mühlbauer, B. Binz, F. Jonietz, C. Pfeleiderer, A. Rosch, A. Neubauer, R. Georgii, and P. Böni, Science **323**, 915 (2009).
- [6] X. Z. Yu, Y. Onose, N. Kanazawa, J. H. Park, J. H. Han, Y. Matsui, N. Nagaosa, and Y. Tokura, Nature **465**, 901 (2010).
- [7] G. Gervais, H. L. Stormer, D. C. Tsui, P. L. Kuhns, W. G. Moulton, A. P. Reyes, L. N. Pfeiffer, K. W. Baldwin, and K. W. West, Phys. Rev. Lett. **94**, 196803 (2005).
- [8] G. E. Volovik, *The Universe in a Helium Droplet* (Clarendon Press, Oxford, 2003).
- [9] M. Ichioka, T. Mizushima, and K. Machida, Phys. Rev. B **82**, 094516 (2010).
- [10] J.-Y. Choi, W. J. Kwon, and Y.-I. Shin, Phys. Rev. Lett. **108**, 035301 (2012).
- [11] Y. Brihaye, C. T. Hill, and C. K. Zachos, Phys. Rev. D **70**, 111502 (2004) and references therein.
- [12] U. A. Khawaja and H. T. C. Stoof, Nature (London) **411**, 918 (2001).
- [13] U. A. Khawaja and H. T. C. Stoof, Phys. Rev. A **64** 043612 (2001).
- [14] J. Ruostekoski and J. R. Anglin, Phys. Rev. Lett. **86** 3934 (2001).
- [15] R. A. Battye, N. R. Cooper, and P. M. Sutcliffe, Phys. Rev. Lett. **88** 080401 (2002).
- [16] C. M. Savage and J. Ruostekoski, Phys. Rev. Lett. **91** 010403 (2003).
- [17] S. Wüster, T. E. Argue, and C. M. Savage, Phys. Rev. A **72**, 043616 (2005).
- [18] I. F. Herbut and M. Oshikawa, Phys. Rev. Lett. **97**, 080403 (2006).
- [19] A. Tokuno, Y. Mitamura, M. Oshikawa, and I. F. Herbut, Phys. Rev. A **79**, 053626 (2009).
- [20] C. Wang, C. Gao, C.-M. Jian, and H. Zhai, Phys. Rev. Lett. **105**, 160403 (2010).
- [21] T. Kawakami, T. Mizushima, and K. Machida, Phys. Rev. A **84**, 011607(R) (2011).
- [22] J. M. Gipson and H. C. Tze, Nucl. Phys. **B183**, 524 (1981).
- [23] Y.-J. Lin, R. L. Compton, A. R. Perry, W. D. Phillips, J. V. Porto, and I. B. Spielman, Phys. Rev. Lett. **102**, 130401 (2009).
- [24] Y.-J. Lin, R. L. Compton, K. Jimenez-Garcia, J. V. Porto, and I. B. Spielman, Nature (London) **462**, 628 (2009).
- [25] Y.-J. Lin, K. Jiménez-Garcia, and I. B. Spielman, Nature (London) **471**, 83 (2011).
- [26] J. P. Vyasankere, S. Zhang, V. B. Shenoy, Phys. Rev. B **84**, 014512 (2011).
- [27] M. Gong, S. Tewari, C. Zhang, Phys. Rev. Lett. **107**, 195303 (2011).
- [28] H. Zhai, Int. J. Mod. Phys. B **26**, 1230001 (2012) and references therein.
- [29] G. Juzeliūnas, J. Ruseckas, and J. Dalibard, Phys. Rev. A **81**, 053403 (2010).
- [30] D. L. Campbell, G. Juzeliūnas, I. B. Spielman, Phys. Rev. A **84**, 025602 (2011).
- [31] B. M. Anderson, G. Juzeliūnas, I. B. Spielman, and V. M. Galitski, Phys. Rev. Lett. **108** 235301 (2012).
- [32] J. Ruseckas, G. Juzeliūnas, P. Öhberg, and M. Fleischhauer, Phys. Rev. Lett. **95**, 010404 (2005).
- [33] T. Mizushima, K. Machida, and T. Kita, Phys. Rev. A **66**, 053610 (2002) and references therein.
- [34] K. Kasamatsu, M. Tsubota, and M. Ueda, Phys. Rev. A **71**, 043611 (2005).
- [35] R. L. Davis and E. P. S. Shellard, Nucl. Phys. B **323**, 209 (1989).
- [36] H. Hu, B. Ramachandhran, H. Pu, X.-J. Liu, Phys. Rev. Lett. **108**, 010402 (2012).
- [37] S.-W. Su, I.-K. Liu, Y.-C. Tsai, W. M. Liu, S.-C. Gou, arXiv:1111.6338.
- [38] E. Babaev, L. D. Faddeev, and A. J. Niemi, Phys. Rev. B **65**, 100512(R) (2002).
- [39] Y. Kawaguchi, M. Nitta, and M. Ueda, Phys. Rev. Lett. **100**, 180403 (2008).
- [40] Y. Li, X. Zhou, and C. Wu, arXiv:1205.2162.
- [41] B. M. Anderson and C. W. Clark, arXiv:1206.0018.